Clays and Clay Minerals, Vol. 56, No. 1, 23–38, 2008.

GEOCHEMICAL RECORDS OF A BENTONITIC ACID-TUFF SUCCESSION RELATED TO A TRANSGRESSIVE SYSTEMS TRACT – INDICATION OF CHANGES IN THE VOLCANIC SEDIMENTATION RATE

Z. Püspöki[1,*], M. Kozák[1], P. Kovács-Pálffy[2], J. Szepesi[1], R. McIntosh[1], P. Kónya[2], L. Vincze[1], and G. Gyula[1]

[1] Department of Mineralogy and Geology, University of Debrecen, Egyetem tér 1., Debrecen, H-4032, Hungary
[2] Geological Institute of Hungary, Stefánia út 14., Budapest, H-1142, Hungary

Abstract—A detailed stratigraphic and facies reconstruction of a bentonitized acid-tuff succession, deposited within the transgressive systems tract of the Upper Miocene–Sarmatian Ser-3 eustatic cycle, at Sajóbábony, northern Hungary, was performed *via* petrographic, mineralogical and geochemical analyses. The purpose of the work was to analyze the degree of alteration of the volcanogenic sediments, as an indicator of the relative volcanic sedimentation rate. This may have an important role in indicating volcanic periods synchronous with sedimentation or reconstructing the volcanosedimentary paleoconditions. Sample pairs were collected from each bentonite and tuff layer, and, to facilitiate microstratigraphic relations, samples were collected every 10 cm within bentonite layers. Mineralogical analyses were performed by X-ray diffraction and geochemical analyses by inductively coupled plasma-mass spectroscopy.

The CaO/K_2O and Eu/La ratios correlate with each other and with a montmorillonite/X-ray-amorphous phase ratio, reflecting Ca and Eu incorporation associated with devitrification and smectite formation. In accordance with the current literature, these mineralogical and geochemical proxies can be related primarily to the weathering processes. Considering vertical distributions in a sequence-stratigraphic context, the Ca content and Eu/La values show that local peaks and Eu anomalies characteristic of acid tuffs show minima at flooding surfaces (FS). Within a bentonite layer, representing a single transgressive period, the repeated events of dust-tuff accumulations have been determined by K_2O/CaO and La/Eu peaks, confirmed also by the Eu anomalies in the rare earth element (*REE*) patterns, thus leading to the conclusion that the level of alteration is closely correlated with the elimination of terrigenous input and a minimum in volcanic sedimentation rate allowing more intensive alteration of the deposited volcanic material. In the case of fine tuff beds, Eu anomalies on *REE* patterns reflect limited alteration at the bottom and more intensive alteration in the upper parts of the beds, reflecting the effect of infiltration of sea water into the pores.

Key Words—Acid-tuff Sedimentation, Bentonites, Geochemistry, Sediment Condensation, Sequence Stratigraphy.

INTRODUCTION

The determination of volcanic rhythms and micro-rhythms using the distal facies of a pyroclastic airfall succession may have great importance for stratigraphic and paleogeographic perspectives, in Cenozoic, Paleozoic, and Mesozoic strata alike, since facies analysis, basin research, and volcanic and palinspastic reconstructions rely equally on the accurate recognition of the volcanic events. Assuming submarine accumulation with a more or less complete preservation, the appearance of the volcanogenic material in sedimentary sequences is controlled by the interaction of episodic volcanic activity and sedimentary processes such as condensed sedimentation during transgression and progradation of terrigenous input.

Episodic occurrence of volcanic activity simultaneously with a eustatic transgression is a rare but not unique situation. Sediment condensation during transgression may shut off terrigenous input into the system, resulting in exclusive deposition of airfall volcanic ash, depending on the rate of tuff fall relative to changes in accommodation space. Relatively short periods of low to no net ash deposition may enable the weathering of the volcanic material and thus the consequent formation of smectite. The bentonite layers forming in this way, as confirmed mineralogically by using flooding surfaces, are useful key beds in geophysical, *i.e.* well-to-well correlations and sequence stratigraphic reconstructions (Cant, 1992). However, even under these relatively homogeneous conditions, a variation in the level of alteration can be assumed related to the changes in the volcanic sedimentation rate. The periods of decreased volcanic input allow for greater alteration, while greater tuff accumulation can inhibit weathering; therefore detailed analysis of the alteration may indicate changes in volcanic sedimentation rate.

Analysis of early diagenetic alteration of volcanic glass in volcanogenic sediments requires conventional petrographic, sedimentological, mineralogical, and geochemical data. However, in numerous cases, the limits of petrological and/or sedimentological methods enhance

* E-mail address of corresponding author:
puspokiz@gmail.com
DOI: 10.1346/CCMN.2008.0560103

the role of mineralogical and geochemical data (*e.g.* Kolata *et al*., 1998; Bergström *et al*., 1998; Huff *et al*., 2000; Min *et al*., 2001; Ver Straeten, 2004).

In the course of an economic geological exploration of a Sarmatian, Upper Miocene bentonite locality in Sajóbábony, northern Hungary (Figure 1), significant changes in montmorillonite content were detected. The vertical distribution and lithological relationships of the altered volcanic material appear to indicate an association with stratigraphic position and sedimentary conditions during development of a transgressive systems tract. The aims of this paper are: (1) to distinguish the development of small-scale cycles in purely tuff sediments, which were deposited within a transgression/transgressive systems tract; (2) to test some associated mineralogical and geochemical data as indicators/proxies of the degree of alteration of the volcanic material; and (3) to investigate the control of the relative rate of volcanic sedimentation on the degree of alteration.

PALEOGEOGRAPHIC AND STRATIGRAPHIC POSITION OF THE SERIES

The Borsod Basin of Hungary, at the time at which the bentonitic succession of interest was deposited, was a relatively emerged marginal sub-basin of the Central Paratethys in the Miocene (Figure 1). Thus the early lowstand systems tracts (LST) of the Miocene 3rd order sedimentary cycles in the region, including a sequence comprising the upper part of the Sajó Valley Fm., were represented by sub-aerial denudation and the formation of unconformities. Sea water flooded the area during the transgressive systems tracts (TST) (Figure 2). Much of the highstand systems tracts (HST) of each sequence was eroded during subsequent LSTs. Therefore, the sequences consist primarily of TSTs and early HSTs, separated by significant unconformities (Püspöki, 2002).

Stratigraphic and lithological data indicate that the pyroclastic deposits, which are the focus of this study, represent distal airfall deposits of episodic Sarmatian rhyolitic volcanism, which accumulated within a TST. Based on the macrofauna data from the overlying sediments, this TST is part of the Ser-3 depositional sequence (Vakarcs *et al.*, 1998) (Figure 2). Püspöki *et al.* (2005) demonstrated that the accumulation of the pyroclastic sediments was the result of the interaction between the volcanic activity and transgression-related processes. The former provided the bulk of sediments during the transgression, while the latter influenced the deposition and preservation of the tuffaceous material.

METHODS

The bentonite-bearing strata have been explored using 27 deep drillings, 21 of which feature continuous

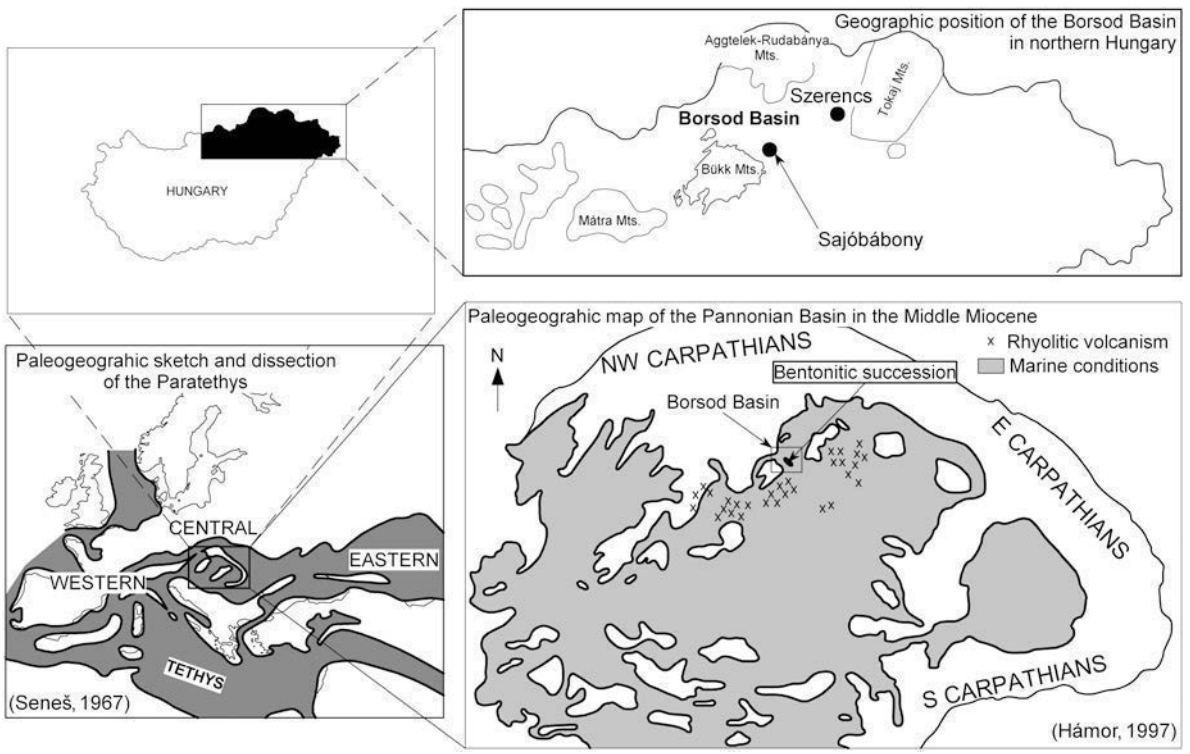

Figure 1. Geographic location and paleogeographic situation of the Borsod Basin and the bentonitic succession at Sajóbábony, in Central Paratethys, Pannonian Basin terms.

https://doi.org/10.1346/CCMN.2008.0560103 Published online by Cambridge University Press

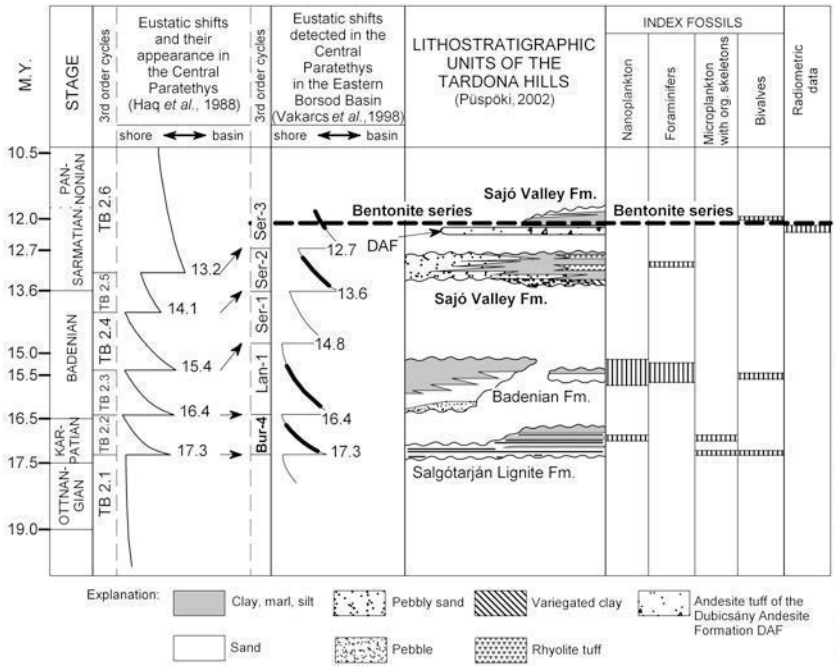

Figure 2. Stratigraphic position of the bentonite series according to the eustatic shifts of the Central Paratethys and the Borsod Basin.

core samples. Well logs of boreholes SZPKF-1, SZPKF-2, SZPKF-3, SZPKF-5, SZPKF-11, and SZPKF-RK-5 were correlated with each other (Figure 3) and with natural exposures in the neighboring Kő valley. Core samples were cut and polished to document sedimentary structures.

Mineralogical composition and major, trace, and *REE* elements were determined from bentonite and bentonitic tuff samples taken from the SZPKF-RK-5 core and from Kő valley outcrops. In order to examine the sequence stratigraphic trends of the chemical changes, two samples – a 'lower' and an 'upper' – were taken and analyzed from each bentonite and bentonitic tuff layer. In order to detect the microstratigraphic trends in mineralogical and geochemical changes, samples were taken systematically every 10 cm within bentonite layers.

Determination of the mineralogical composition was performed by XRD analyses on whole-rock samples, using CuKα radiation (40 kV, 30 mA, 2º/min) with a PC-controlled Phillips PW 1730 powder diffractometer equipped with a graphite monochromator. The mineral composition was calculated on the basis of the relative intensities of the characteristic reflections using either literature data or experimental corundum mineral factors (Klug and Alexander, 1954; Náray-Szabó *et al.*, 1965; Rischák and Viczián, 1974; Rischák, 1989). Optical investigations of thin sections were also performed on suitable samples.

The clay mineral content was determined on oriented samples of the fine fraction (<2 μm) and the montmorillonite content was calculated in two different ways for better determination, based on the 001 and 110 reflection intensities using empirical factors 0.7 and 1.5, respectively. This was necessary because for most of the samples the 001 basal reflections were of low intensity and diffuse but the 110 reflections were of acutely high intensity.

Geochemical components as major, trace, and *REE* elements were investigated at the Geological Institute of Hungary (Bartha *et al.*, 2004). The major and trace elements of rock samples were determined using the lithium metaborate decomposition method of Bertalan *et al.* (2003).

The major components, *i.e.* SiO_2, TiO_2, Al_2O_3, Fe_2O_3, MnO, CaO, MgO, Na_2O, K_2O, P_2O_5, SO_3, BaO, and SrO, were analyzed by inductively coupled plasma-optical emission spectroscopy (ICP-OES) using a JY ULTIMA 2C ICP-OES instrument after a tenfold dilution of the stock solution. The final sample concentration was 0.2 g L^{-1}. The FeO was determined by titration with $KMnO_4$ after gentle sample decomposition, while the CO_2 content was determined by a gas volumetric method with a 0.02% detection limit. The $-H_2O$ and $+H_2O$ contents were determined by gravimetric methods with a 0.01% detection limit value.

Some trace elements, *i.e.* Co, Cr, Cu, Ni, V, and Zn, were also determined by ICP-OES. The analysis was performed on the original stock solution. The rest were determined by inductively coupled plasma-mass spectrometry (ICP-MS) using a VG PlasmaQuad II STE ICP-MS instrument (according to Bartha and Bertalan, 1997). The final sample concentration was 0.2 g L^{-1}. For the internal standard for the determination, 10 mg/kg ^{115}In was used. The detection limits and analytical uncertainty

https://doi.org/10.1346/CCMN.2008.0560103 Published online by Cambridge University Press

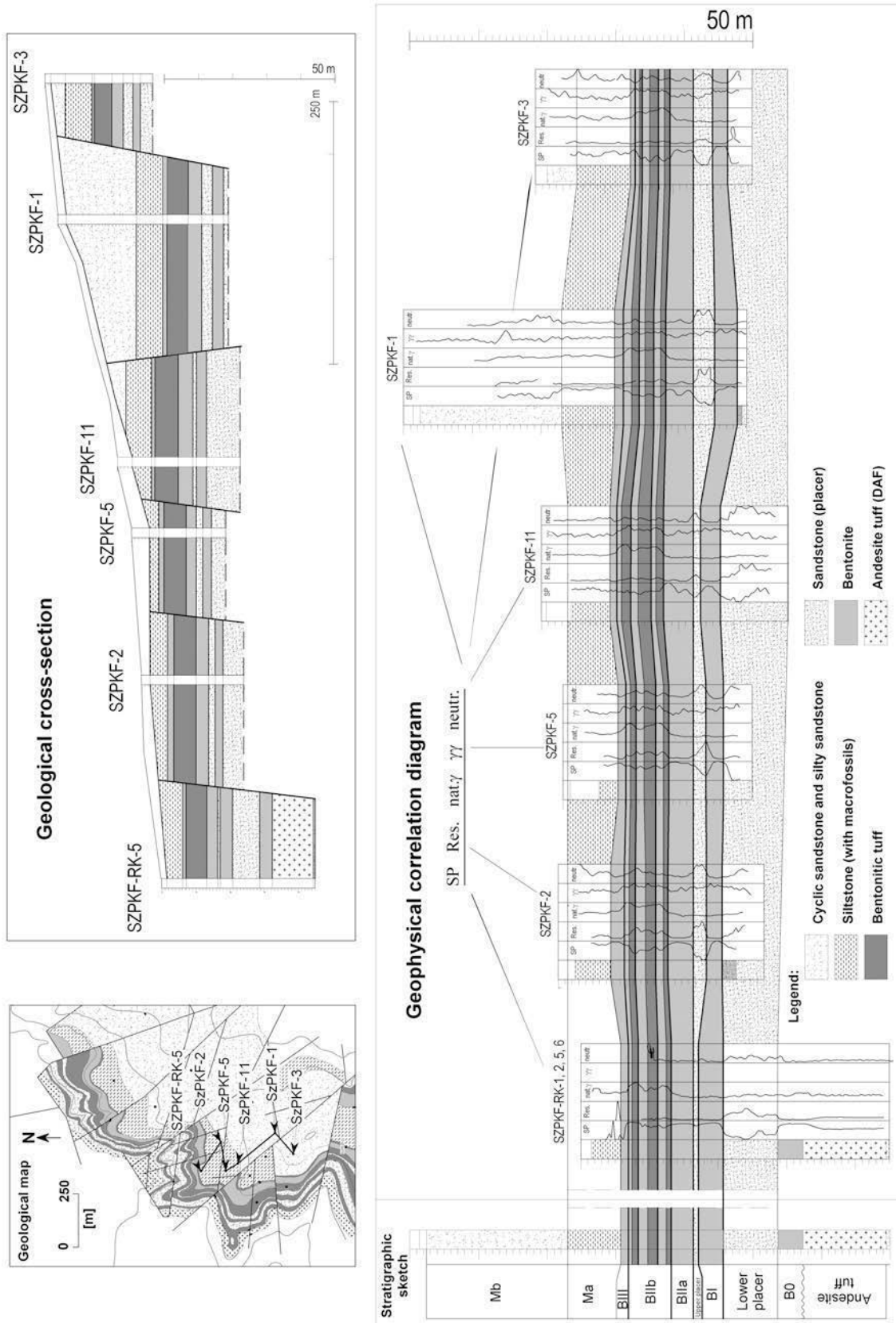

Figure 3. Geological map, cross section and geophysical correlation diagram of the bentonitic succession at Sajóbábony.

https://doi.org/10.1346/CCMN.2008.0560103 Published online by Cambridge University Press

achieved by the applied methods (Juvonen *et al.*, 2004) are given in Tables 1–3 deposited at: http://www.clays.org/journal/JournalDeposits.html.

RESULTS

Stratigraphic and facies description

The strata which are the focus of this study unconformably overlie a geographically widespread andesite tuff, the Dubicsány Andesite Formation (DAF). In borehole SZPKF-RK-5 and in the natural outcrop of the Kő valley, a thin (<40 cm thick), pumiceous tuff lies directly on the eroded surface of the DAF (Figure 4). Noting its rhyolite character, in contrast to the underlying andesite tuff, and its affinity with the acidic character of the subsequent volcanogenic sediments, this pumiceous layer is termed 'base tuff'.

The first bentonite layer, termed 'B0' is 2–3 m thick. This bed was deposited directly on the base tuff as in the SZPKF-RK boreholes and Kő valley. The B0 bentonite layer is overlain by 5–6 m of sand-rich sediments representative of a prograding shoreline, termed the 'lower placer'. Upward increasing energy of this parasequence is indicated by both reworked bentonitic clasts from the underlying beds (figure 6b in Püspöki *et al.*, 2005) and dominantly oblique to vertical trace fossils and incomplete bioturbation of the strata by suspension-feeding organisms (figure 6c in Püspöki *et al.*, 2005).

The second parasequence starts with a bentonite layer, labeled 'BI', 2–2.5 m thick. It is characterized by micrograded bedding, indicative of submarine accumulation within low-energy paleoenvironments, where sediment accumulation was episodic (Figure 5a). The episodic character of the accumulation may also be indicated by alternating degrees of bioturbation of the strata reflecting fluctuation in depositional rates or environmental conditions, the availability of food sources in sediments, *etc*. (figure 6d in Püspöki *et al.*, 2005). The BI layer is covered by sandy shoreline sediments, no thicker than 2 m on average. This sandy facies, termed the 'upper placer', is similar to the 'lower placer', with an arkosic, subarkosic, or placer character and abundant pyroxene, indicative of a short transport distance.

The third bentonite layer, marked as 'BIIa' is nearly 4 m thick. It is yellowish green, poorly bedded to non-bedded, fine sandy silt in terms of grain size, sometimes with scattered pumice fragments. Bed surfaces, when visible, are uneven. The frequent appearance of some minerals, such as quartz, with undulating extinction, and of small crystals of muscovite, visible in thin sections, reflects the mixing of volcanogenic and reworked siliciclastic sediments. Separate clay mineral nodules can also be seen.

The BIIb unit is dominantly a coarse vitroclastic tuff. The pyroclastic fragments, comprising 75–100%, are dominantly vitroclasts, such as volcanic glass and pumice fragments. The pumice fragments are 1–2 mm in diameter; thus the material may be termed lapilli tuff. Considering the dominant size of the particles, the frequency of the pumice fragments and some special sedimentary features detailed below, the BIIb unit can be subdivided into six sub-units. These are illustrated in Figure 5. A detailed description of the matrix related to the type and alteration; the size, form and alteration of the enclosed pumices and lapilli; the sedimentological description of the intraclasts and interbedding material;

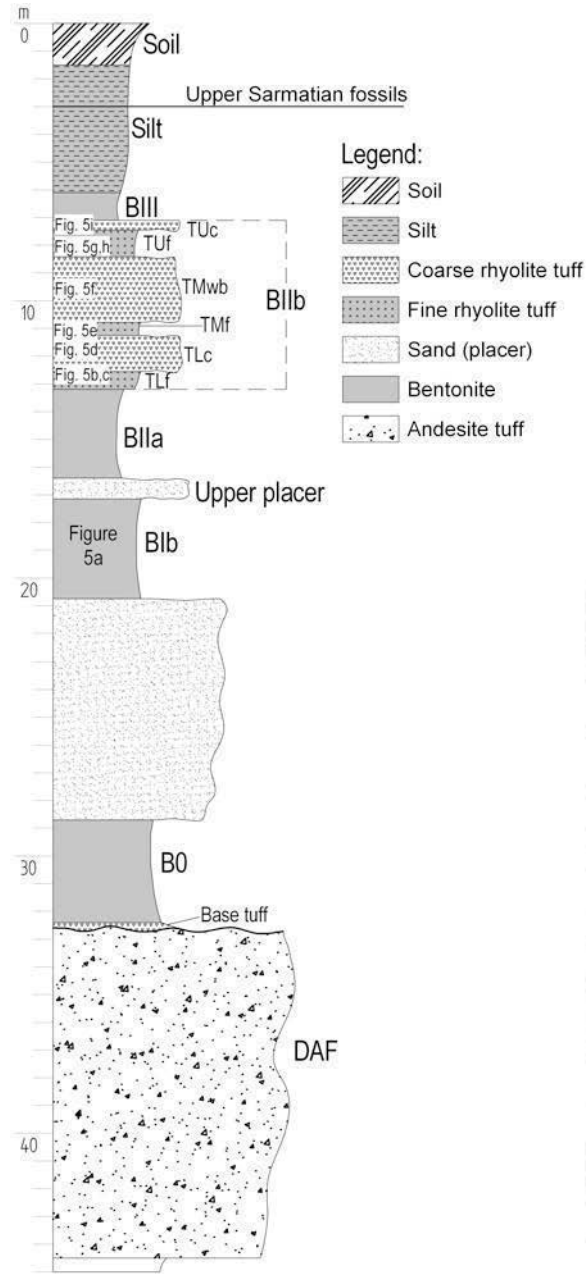

Figure 4. Stratigraphic outline of the bentonitic tuff succession with the relative positions of slabs presented in Figure 5.

https://doi.org/10.1346/CCMN.2008.0560103 Published online by Cambridge University Press

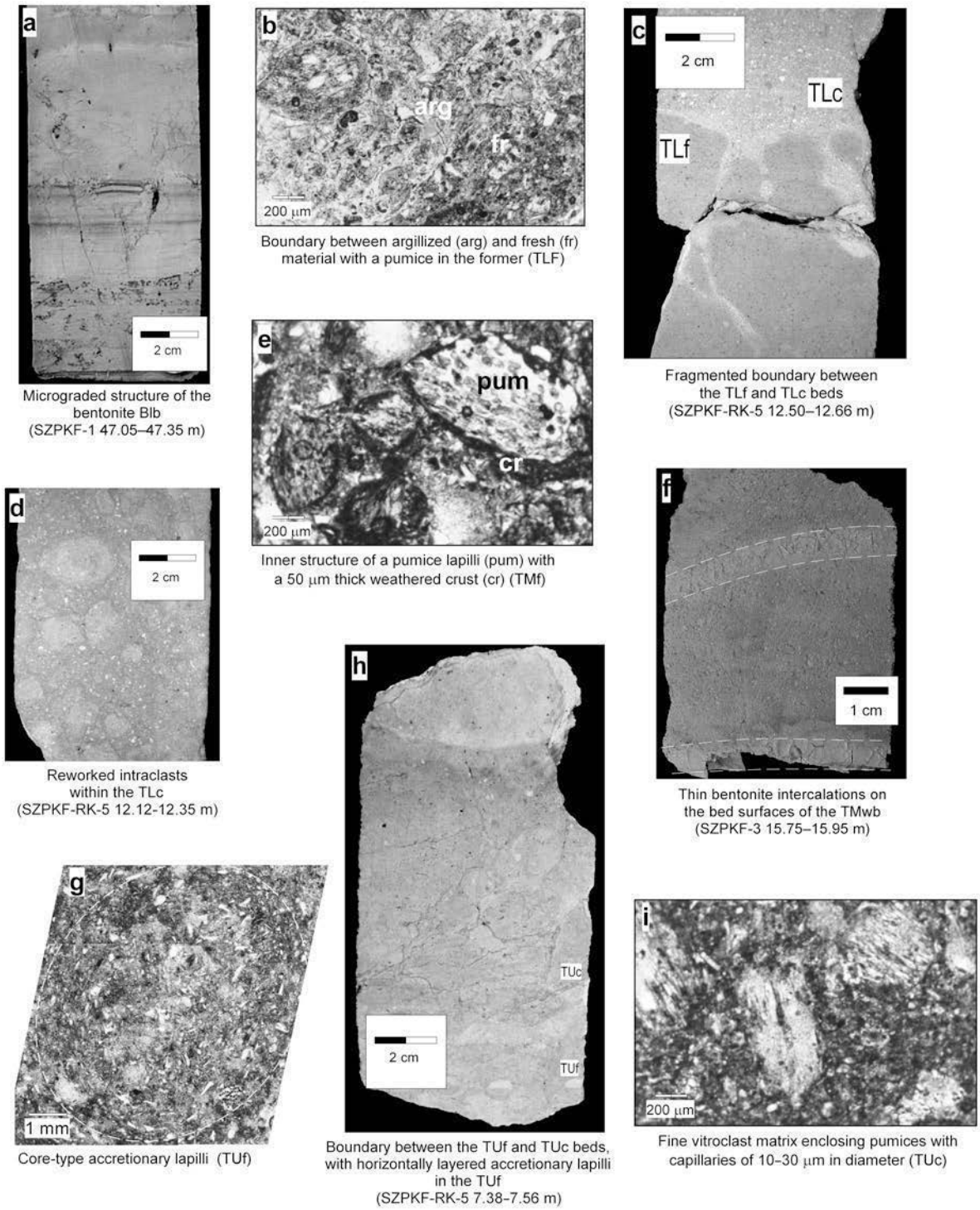

Figure 5. Characteristic features of the bentonite and bentonitic tuff beds of the succession.

and the types, shapes, and sizes of the crystals is given in Figure 6.

The lower, finer tuff sub-unit ('TLf' for Tuff Lower fine) of the BIIb tuff is <1 m thick and the material contains small intraclasts with different levels of argillization (Figure 5b). The upper bed surface is strongly cracked, and the fissures are filled with material from the overlying rhyolite tuff (Figure 5c). The strongly weathered material of the overlying lower coarser tuff sub-unit ('TLc' for Tuff Lower coarse) is

https://doi.org/10.1346/CCMN.2008.0560103 Published online by Cambridge University Press

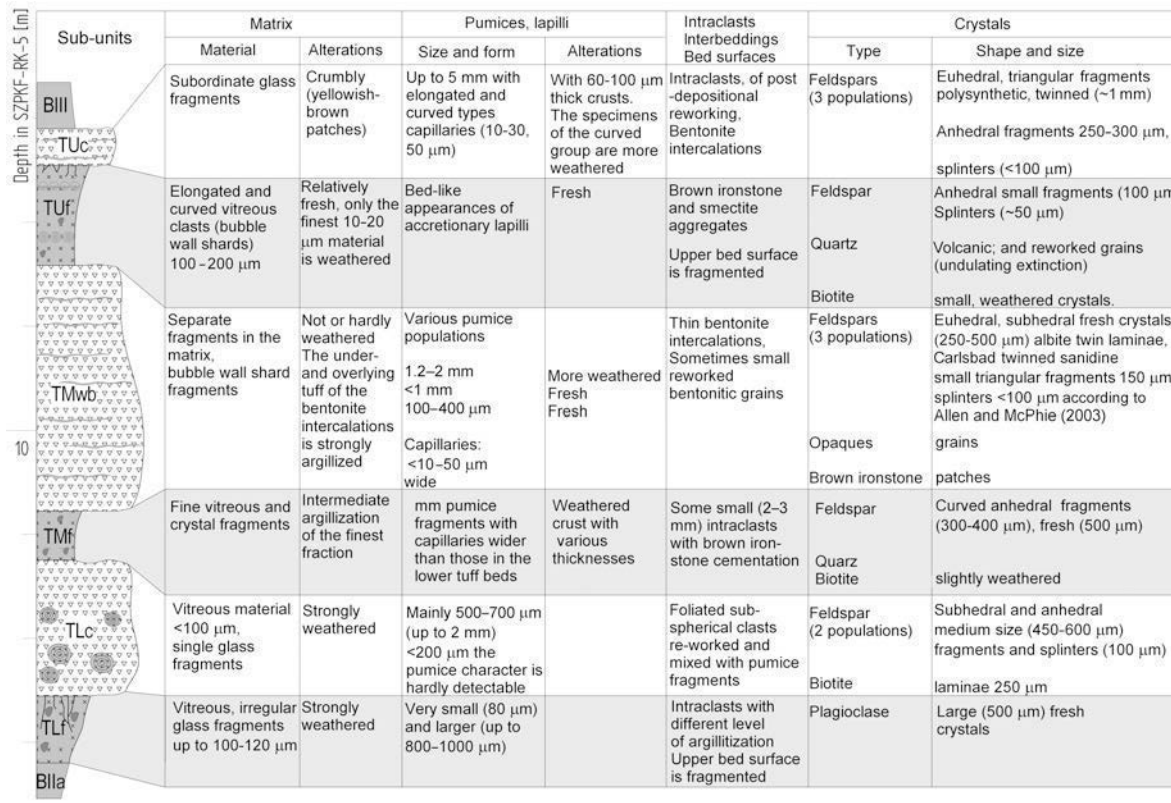

Sub-units	Matrix		Pumices, lapilli		Intraclasts Interbeddings Bed surfaces	Crystals	
	Material	Alterations	Size and form	Alterations		Type	Shape and size
BIII TUc	Subordinate glass fragments	Crumbly (yellowish-brown patches)	Up to 5 mm with elongated and curved types capillaries (10-30, 50 μm)	With 60-100 μm thick crusts. The specimens of the curved group are more weathered	Intraclasts, of post -depositional reworking. Bentonite intercalations	Feldspars (3 populations)	Euhedral, triangular fragments polysynthetic, twinned (~1 mm) Anhedral fragments 250-300 μm, splinters (<100 μm)
TUf	Elongated and curved vitreous clasts (bubble wall shards) 100 - 200 μm	Relatively fresh, only the finest 10-20 μm material is weathered	Bed-like appearances of accretionary lapilli	Fresh	Brown ironstone and smectite aggregates Upper bed surface is fragmented	Feldspar Quartz Biotite	Anhedral small fragments (100 μm) Splinters (~50 μm) Volcanic; and reworked grains (undulating extinction) small, weathered crystals.
TMwb	Separate fragments in the matrix, bubble wall shard fragments	Not or hardly weathered The under- and overlying tuff of the bentonite intercalations is strongly argillized	Various pumice populations 1.2–2 mm <1 mm 100–400 μm Capillaries: <10–50 μm wide	More weathered Fresh Fresh	Thin bentonite intercalations. Sometimes small reworked bentonitic grains	Feldspars (3 populations) Opaques Brown ironstone	Euhedral, subhedral fresh crystals (250-500 μm) albite twin laminae, Carlsbad twinned sanidine small triangular fragments 150 μm splinters <100 μm according to Allen and McPhie (2003) grains patches
TMf	Fine vitreous and crystal fragments	Intermediate argillization of the finest fraction	mm pumice fragments with capillaries wider than those in the lower tuff beds	Weathered crust with various thicknesses	Some small (2–3 mm) intraclasts with brown iron-stone cementation	Feldspar Quarz Biotite	Curved anhedral fragments (300-400 μm), fresh (500 μm) slightly weathered
TLc	Vitreous material <100 μm, single glass fragments	Strongly weathered	Mainly 500–700 μm (up to 2 mm) <200 μm the pumice character is hardly detectable		Foliated sub-spherical clasts re-worked and mixed with pumice fragments	Feldspar (2 populations) Biotite	Subhedral and anhedral medium size (450-600 μm) fragments and splinters (100 μm) laminae 250 μm
TLf BIIa	Vitreous, irregular glass fragments up to 100-120 μm	Strongly weathered	Very small (80 μm) and larger (up to 800–1000 μm)		Intraclasts with different level of argillitization Upper bed surface is fragmented	Plagioclase	Large (500 μm) fresh crystals

Figure 6. General characteristics of the sub-unit BIIb.

rich in pumice fragments. In contrast to the underlying sub-unit, the TLc can be termed a lapilli tuff. Foliated, subspherical clasts similar to the material of the TLf can frequently be seen in the TLc lapilli tuff layer (Figure 5d), indicating that the material of previously deposited rhyolite tuff was re-worked and mixed into the overlying tuff sub-unit. Mixing is indicated by the appearance of pumice fragments, characteristic of only the TLc, within the intraclasts.

The matrix of the middle finer tuff sub-unit ('TMf', for Tuff Middle fine), scarcely 0.5 m thick, is cemented by clay minerals and siliceous material. The tuff is characterized by pumice fragments with weathered crust of various thicknesses (Figure 5e). The material of the middle well-bedded sub-unit ('TMwb', for Tuff Middle well bedded) is similar to the lapilli tuff of the TMf. The TMwb appears well bedded, with undulating bedding surfaces. Thin bentonite intercalations within the TMwb occur frequently along the bedding surfaces (Figure 5f). Euhedral feldspar crystals and pumice fragments occur sparsely in the bentonite layers. Tuffaceous layers below and above the bentonitic intercalations are strongly argillized, containing two populations of pumice fragments, fresh ones of <1 mm and more weathered ones of 1.2–2 mm diameter. The material may result from a number of thin accumulations of tuff deposited over time, which may then have been reworked by marine processes such as storms, currents, or tides. During breaks in tuff deposition or re-deposition, the sorted fine fractions may have been reworked, forming the thin bentonite intercalations.

The material of the upper finer tuff sub-unit ('TUf', for Tuff Upper fine) appears as a thin-bedded, nearly laminar rhyolite tuff, with non-parallel bedding surfaces. The TUf bed is also characterized by a bed-like distribution of accretionary lapilli, 5–12 mm in diameter, formed as a result of collisions between liquid-coated particles due to terminal fall velocity differences in eruption plumes. Both concentric and hemispherical structures can be observed with finer and darker material in the center, and lighter and coarser material towards the edge as the 'core-type' lapilli (according to Gilbert and Lane, 1994). The concentric distribution of needle-like crystals and vitreous clasts and fine pumiceous fragments are indicative of the noted accretion mechanism (Figure 5g). However, on slabs, lapilli with horizontal layering can also be observed (Figure 5h).

The texture of the upper coarser tuff sub-unit ('TUc', for Tuff Upper coarse) shows similarities with the TMwb. The material is poorly sorted; fine and coarse material is not separated into discrete layers. This is the coarsest tuff in the BIIb unit, with large pumice fragments (Figure 5i). The lower bed surface of the TUc, towards the underlying TUf, is strongly fragmented (Figure 5g). This sub-unit is

https://doi.org/10.1346/CCMN.2008.0560103 Published online by Cambridge University Press

also characterized by intraclasts, indicative of post-depositional reworking. Thin bentonite intercalations and poor bedding can also be seen, reflective of episodic breaks in tuff accumulation.

The 'BIII' bentonite layer was deposited on top of the BIIb bentonitic tuff unit. It appears as a relatively thin bed of montmorillonite-rich greenish grey silty clay, altered from an accumulation of volcanic ash. The most characteristic sedimentary features of the layer are carbonate concretions, usually <5 mm in diameter, but sometimes having a diameter of several cm.

Following deposition of the BIII bentonite layer, mixed clastic and carbonate sediments with marine fossils became dominant. They reach a thickness of up to 10 m. Well preserved index fossils of Upper Sarmatian age are present in the lower part of the interval.

The overlying succession is characterized by generally coarsening-up, cyclic sedimentation of sandy siltstone and fine sandstone. This is interpreted to represent a lower shoreface paleo-environment, with the dominance of sandy shoreface facies gradually increasing upwards.

Mineralogical composition

Mineralogical compositions of all bentonite and tuff samples were determined from borehole SZPKF-RK 5 and from one selected core sample of SZPKF-1. The mineralogical compositions of the samples are listed in Table 1 (deposited at: http://www.clays.org./journal/JournalDeposits.html).

A strong opposing trend between montmorillonite and the X-ray-amorphous phase is confirmed by their relatively strong negative correlation with $R^2 = 0.66$ and related to the degree of alteration of the material. Large concentrations of montmorillonite are observed within the B0, BI, BIIa, and BIII layers, with minimum concentrations in the TLf, TMf, and TUf layers, reflecting greater and lesser degrees of weathering, respectively. An apparent correlation between the X-ray amorphous phase and K-feldspar, which is not confirmed by a significant positive correlation with $R^2 = 0.4$, reflects their common tuffaceous origin. Similarly weak, with $R^2 = 0.4$, and extremely weak, with $R^2 = 0.009$, correlations between montmorillonite and K-feldspar, and montmorillonite and plagioclase feldspar, respectively, can also be observed.

Among clay minerals, montmorillonite is dominant in samples. Illite is found in minor amounts (5–16%), while the kaolinite concentration does not exceed 6%. Their stratigraphic distribution seems to be independent of both montmorillonite and of tuffaceous minerals, which is indicated by the lack of correlation between them with $R^2 = 0.0003$ and 0.13, respectively.

Geochemical characteristics

Stratigraphic trends of the chemical elements were examined. Considering their vertical distribution, some elements (Tables 2 and 3, deposited at: http://www.clays.org/journal/JournalDeposits.html) group together, show correlative trends through the succession, and appear to be related to different processes active in the depositional system. One group of elements, which includes various major, trace, and *REE* elements, shows relatively significant concentrations in the B0, BI, BIIa, TMwb, and BIII layers. These elements are Ca, Mg, Sr, and Eu. Tantalum and Nb decrease in concentration from B0 to BIIa while K, U, and Rb also decrease from TLf to TMwb and from TUf to BIII. The stratigraphic distribution of immobile *REE* elements from La to Lu and Y, excluding Eu, seems to be independent of the first and second groups. Spider diagrams of *REE* elements have been created to detect stratigraphic changes in *REE* concentrations. The most important relationships, together with interpretations, will be given below.

DISCUSSION

Sedimentary cycles and sedimentological aspects of the synsedimentary volcanism

The whole bentonite-bearing succession in the upper part of the Sajó Valley Fm. was developed by the interaction of sedimentary processes active during the TST of the Ser-3 eustatic cycle the age of which is 12.7 Ma (Vakarcs *et al.*, 1998) and explosive, Upper Miocene rhyolite tuff volcanism with radiometric ages ranging from 12.9 to 12.1 Ma (Püspöki *et al.*, 2005). Upwards decreasing thicknesses of the parasequences from the prograding sandstones, represented by the lower and upper placer beds, to the deepest-water facies in the mollusc-bearing siltstones indicate that the bentonite-bearing part of the succession, from the erosive base to the BIII layer, can be regarded as a retrograding parasequence set of a TST. Based on sedimentological characteristics, flooding surface (FS) horizons of individual parasequences coincide with the B0, BI, BIIa, and BIII layers.

The BIIb unit represents a dense tuff accumulation synchronous with the upper part of the TST. The dissection of the unit into 'coarse' and 'fine' sub-units is based on microscopic investigations. In the underlying 'fine' sub-units such as the TLf, TMf, and TUf, pumices seldom reach 1 mm, feldspar populations do not show polymodal character, and their shape is generally anhedral. However, occasionally, *e.g.* in the TLf, large intact feldspars are observed. In contrast, the 'coarse' sub-units such as the TLc, TMwb, and TUc, are characterized by pumices of 2–5 mm in diameter and by two or three populations of feldspar crystals, the largest of which has a diameter of 0.5–1 mm with sub- or euhedral form, while the smallest contains fragments and splinters.

In both 'fine' and 'coarse' sub-units, the fine fraction is no larger than 100–200 μm or the finest one of ~10–20 μm of the vitreous matrix is strongly weathered.

https://doi.org/10.1346/CCMN.2008.0560103 Published online by Cambridge University Press

Some of the pumice fractions are also weathered. Moreover, clayey and brown ironstone encrustation on the pumices is also a common feature, although sometimes fresh pumice specimens or even generations also appear in the material. Thin bentonite intercalations within the beds, *e.g.* in the TMwb and TUc, represent the greatest level of alteration, indicating breaks in tuff accumulation or re-accumulation within a given subunit. Tuff material over- and underlying the bentonite intercalations within the subunits are also usually more weathered than the overall bed.

Regardless of the fine or coarse character of the subunit, several sedimentary features indicate sedimentary reworking and mixing of ash sediments, *e.g.* bh wave, tide, current, or storm. The pumice populations of differing size in the TMwb, and shape in the TUc, represent different levels of alteration. Traces of intensive weathering are observed in only one of the pumice populations such as the largest group in the TMwb and the curved specimens in the TUc, indicating that part of the material is older and more weathered, and thus can be interpreted as a re-deposited fraction. Other features indicative of reworking are the common occurrence of intraclasts throughout the unit, and the presence of reworked, consolidated clasts from underlying tuff subunits. Usually there are apparent differences in the level of argillization which, according to the microscopic data, shows that the reworked material represents the more weathered part of the sample such as smectite aggregates and grains. The third characteristic sedimentary feature of the unit, reflecting a preceding or syn-eruptive cracking of the consolidated tuffaceous bottom, is the appearance of the 'neptunian dykes' at the boundary of sub-units, *e.g.* in the case of the TLf/TLc and TUf/TUc, filled with the material of the subsequent sub-unit.

Possible source, distance, and age of the eruptions

The large concentrations of Rb and K, confirmed by the strong connection between the K and the X-ray amorphous phase, is interpreted to represent feldspar fractionation reflecting late fluid contamination in the magma chamber of the upper crust (Bea, 1996). The high concentrations of incompatible elements such as U, Th, Ta, and *REE* can be explained by the highly fractionated rhyolitic character of the melt (Pearce *et al.*, 2004) and/or, considering also the distal character of the tuff sequence, by the sedimentary separation of the volcanic glass depending on the distance of air transportation (Fisher and Schmincke, 1984).

A special feature of the TUf, related to the distance of the explosion center, is the appearance of accretionary lapilli. The build up of concentric grain-size zones results from differences in the supply of particular grain sizes to the evolving accretionary lapilli, while the existence of horizontally layered lapilli reflects scavenging of particles by liquid drops probably falling as mud rain (Gilbert and Lane, 1994). Considering the appearance of accretionary lappilli accumulated in well defined horizons in the material, the center of explosion might not have been too far from the study area, even in the case of the fine tuffs.

The exact source of the bentonites and tuffs in the sedimentary succession cannot be determined unambiguously and more than one source can be assumed, but worth noting is that the age (12.1 Ma) of the rhyolite volcanism at Szerencs at the southwestern edge of the Tokaj Mts. (see Figure 1) (Pécskay *et al.*, 1987) and the age (12.8±0.5 Ma) of the rhyolite tuff near Szerencs ('Bodrogkeresztur, Kakas Hill' in Pécskay and Molnár, 2002) coincide well with the biostratigraphically defined age of the bentonite-bearing sediment series.

Geochemical proxies for the degree of alteration

The appearance of geochemical elements related to the alteration of the volcanic material is determined by the geochemical characteristics of the source material, *i.e.* the source magma, and by the process of alteration. Some of the elements are specific to the igneous origin of the material, while the rest are related to the processes of weathering and montmorillonite formation.

Among major elements, K has the key role in the investigation of acid magmas, as, being an incompatible element in plagioclase, it is concentrated in the melt during the feldspar fractionation (Bea, 1996). However, under sedimentary conditions, K can be regarded as one of the most mobile elements, its concentration decreasing greatly with weathering. Experimental studies of the interactions between artificial sea water and fresh rhyolite and weakly altered dacitic tuff (Yasumasa *et al.*, 2005) indicate that cation transfer occurs during the smectite-forming processes. Initially, dissolution of K from the rocks accompanies incorporation of Mg and Ca from the artificial sea water during both the earlier devitrification stage and the later smectite formation, whereas Ca incorporated with early smectite formation re-dissolves with progressive reaction. The Sr closely follows Ca because it functions as a substitute for Ca.

Among *REE* elements, a strong negative Eu anomaly in acidic volcanics is also related to the fractionate differentiation of feldspar in the acidic magma (Bea, 1996). This is due to the fact that its partition coefficient (K) to plagioclase and K-feldspar differs by an order of magnitude from those of other *REE* elements, *e.g.* $K_{d\,Eu}^{plag/melt} = 5.14$, contrary to $K_{d\,La}^{plag/melt} = 0.38$ and $K_{d\,Ce}^{plag/melt} = 0.267$ or similarly, $K_{d\,Eu}^{K\text{-}spar/melt} = 2.6$, contrary to $K_{d\,La}^{K\text{-}spar/melt} = 0.072$ and $K_{d\,Ce}^{K\text{-}spar/melt} = 0.046$ (Nash and Crecraft, 1985).

During the chemical alteration of ash in sea water, this inherited negative Eu anomaly gives rise to greater Eu incorporation relative to that of other *REE* elements. In addition, Eu^{3+} substitution for Ca^{2+} has been demonstrated empirically in calcareous, *i.e.* calcite systems (Curti *et al.*, 2005; Lakshtanov *et al.*, 2004) within sea water (Zhong and Mucci, 1995) and under

https://doi.org/10.1346/CCMN.2008.0560103 Published online by Cambridge University Press

alkaline conditions (Tits *et al.*, 2003). The negative Eu anomaly is frequently used as an indicator of the presence of a volcanic component in fine-grained marine sediments (*e.g.* Cullers *et al.*, 1975; Huff *et al.*, 1997a; 1997b; Pellenard *et al.*, 2003); however, due to the high degree of alteration and the effect of diagenesis on Eu enrichment (*e.g.* MacRae *et al.*, 1992), these anomalies are commonly small. A strong negative Eu anomaly in the less weathered tuffs of the BIIb unit, such as the TLf, TMf, and TUf, can clearly be observed, similarly to other unaltered Upper Miocene rhyolite tuffs of the region (Harangi *et al.*, 2005).

Considering these geochemical trends, gradual enrichment in Ca, as opposed to K, can be expected with progressive alteration and bentonitization, together with gradual equalization of the Eu anomaly in the *REE* pattern. This correlation is clearly observable in the study interval in plots of CaO/K_2O *vs.* Eu/La (Figure 7a). Based on data from 52 samples, the correlation is satisfying, with $R^2 = 0.8$, and closer than that between certain elements, *e.g.* CaO *vs.* Eu with $R^2 = 0.67$. The large La concentration, related to that of Eu, is a significant feature in terms of detecting tuffaceous intercalations, so the correlation with reciprocal values of the Eu/La, hereafter La/Eu, is also important ($R^2 = 0.74$). Assuming the gradual disappearance of the negative Eu anomaly until the Eu content of the volcano sediment and of the sea water is equalized, we can calculate the saturation character of the reaction kinetics. Using the $y = Y(1-e^{-Kx})$ formula for the CaO *vs.* Eu values (Figure 7b) (where y is the Eu concentration, Y is the upper limit of Eu concentration; K is the empirical coefficient related to Ca concentration, characteristic of the given ion-exchange reaction; and x is the Ca concentration), the saturation point of the Eu can be calculated as [Eu*] = 1.25 ppm. The parameters of the function have been determined by the Solver function in *MS Excel*®.

Also assuming that the source of the devitrification and smectite formation is the X-ray amorphous phase (Yasumasa *et al.*, 2005), correlation can be expected between the montmorillonite/X-ray amorphous phase and CaO/K_2O, Eu/La (Figure 8a,b), and La/Eu ratios. Data from the borehole SZPKF-RK-5 support this correlation, with $R^2 = 0.59$, $R^2 = 0.72$, and $R^2 = 0.69$, respectively, considering the multiple effects of different methods and the uncertainty of the qualitative determination of the X-ray amorphous phase by XRD. Based on the above correlations, the stratigraphic patterns of the CaO/K_2O and the Eu/La, together with their reciprocal values, confirmed by the associated *REE* patterns, can be regarded as adequate proxies for the level of alteration.

Control of the volcanic sedimentation rate on the level of alteration

The stratigraphic distribution of various sedimentological, petrographic, and geochemical data enables the delineation of sedimentary parasequences within the volcanogenic sediments of the upper part of the Sajó Valley Formation, during the Miocene Ser-3 transgression. Limited accumulation of tuffaceous material at certain levels, leading to greater alteration of ash, together with the progradation of terrigenous material in some intervals, allow detection of the sedimentary

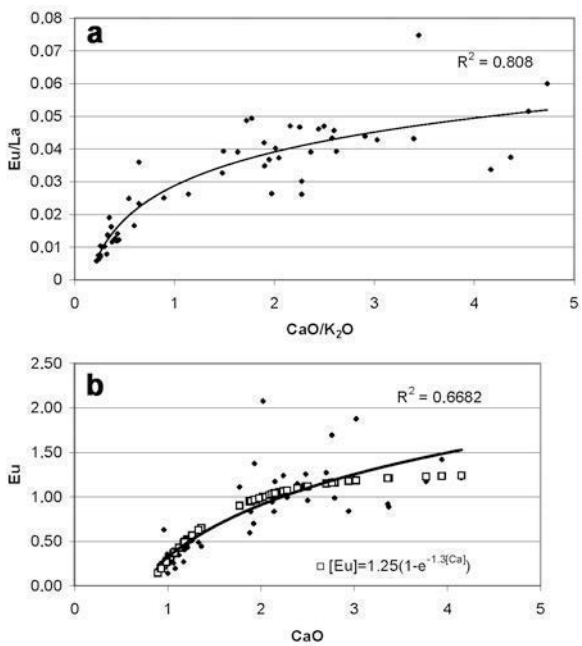

Figure 7. (a) CaO/K_2O *vs.* Eu/La diagram of samples. (b) CaO *vs.* Eu diagram of the samples.

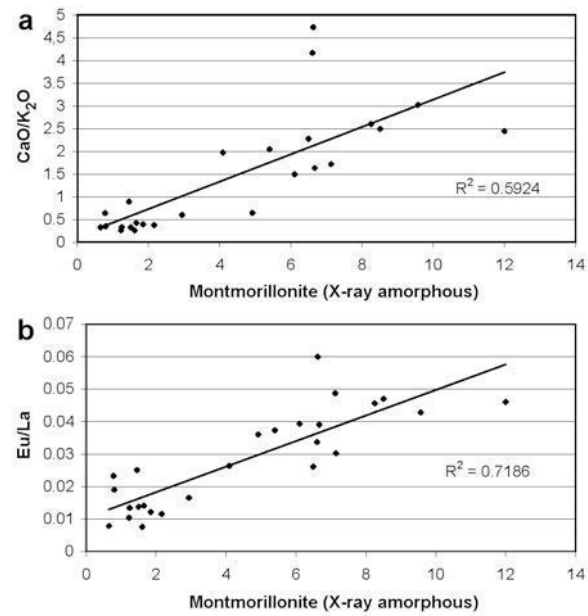

Figure 8. (a) Montmorillonite/X-ray-amorphous phase *vs.* CaO/K_2O diagram of samples. (b) Montmorillonite/X-ray-amorphous phase *vs.* Eu/La diagram of the samples.

https://doi.org/10.1346/CCMN.2008.0560103 Published online by Cambridge University Press

parasequences. In addition, the Ca content and Eu/La values show local peaks (Figure 9), while Eu anomalies (Figure 10) form local minima during flooding periods. These local peaks are related to the elimination of the terrigenous input by transgression and a very limited volcanic sedimentation rate due to the dust-tuff accumulation. This evidence indicates that the B0, BI, and BIIa bentonite layers represent condensed deposits formed on flooding surfaces. The BIII layer is also related to condensed dust-tuff accumulation with a decreased volcanic sedimentation rate and continued limited terrigenous input, this time at the maximum flooding surface (MFS) of the TST.

Detailed analysis of bentonite layers representing a single transgressive period may also have importance from the aspect of the detailed reconstruction of the development and the microstratigraphic dissection of the bentonitic layers. In Figure 11, the geochemical proxies discussed here, *i.e.* Eu/La, La/Eu, and K_2O/CaO values, are plotted together with the associated *REE* patterns. Considering the data, the exact intervals of the condensed volcanic sedimentation at Eu/La peaks and the repeated events of dust-tuff accumulations at La/Eu and K_2O/CaO peaks can be designated, confirmed by the Eu anomalies on the associated *REE* patterns.

Within the BIIb unit, because of the intensive tuff accumulation and the limited amount of the terrigenous material, parasequences are concealed and/or diluted. Based on stratigraphic trends of K_2O/CaO and especially La/Eu ratios, three cycles of tuff accumulation can be detected. Local peaks of these ratios delineate the base of the volcanic rhythms represented by the TLf, TMf, and TUf beds with peaks followed by gradual decreases. The *REE* patterns reflect significant differences in the finer and coarser pumiceous tuffs (Figure 12), since in the TLf, TMf, and TUf, the upper samples are enriched in Eu relative to the lower samples, indicating more intensive alteration at the upper part of the layer, which is interpreted as the result of a limited infiltration of the sea water into the pores of the tuff during the break in sedimentation. In the case of the TLc, TMwb, and TUc, both the lower and upper samples are more altered, reflecting more efficient infiltration of the sea water into the tuffaceous layer. Another interpretation of these phenomena is that within a volcanic cycle ranging from the base of a 'fine' sub-unit to the top of the subsequent 'coarse' sub-unit, a continuous decrease in volcanic sedimentation rate can be detected, *e.g.* due to the increasing accommodation space, associated with the more intensive effect of re-sedimentation.

Identification of cycles of different origin in well-log profiles

The sedimentologically definable flooding events of the B0, BI, BIIa, and BIII layers, together with the subsequent progradation of sand-rich, shallower water

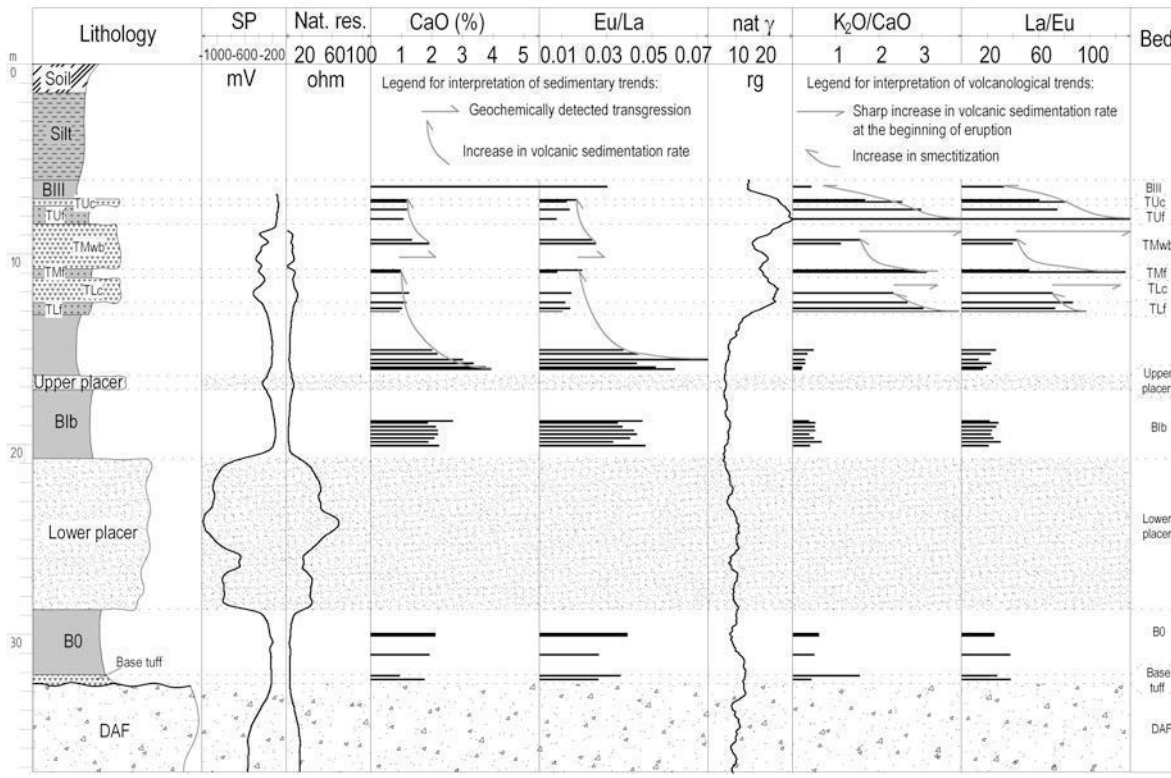

Figure 9. Stratigraphic pattern of the geochemical proxies.

https://doi.org/10.1346/CCMN.2008.0560103 Published online by Cambridge University Press

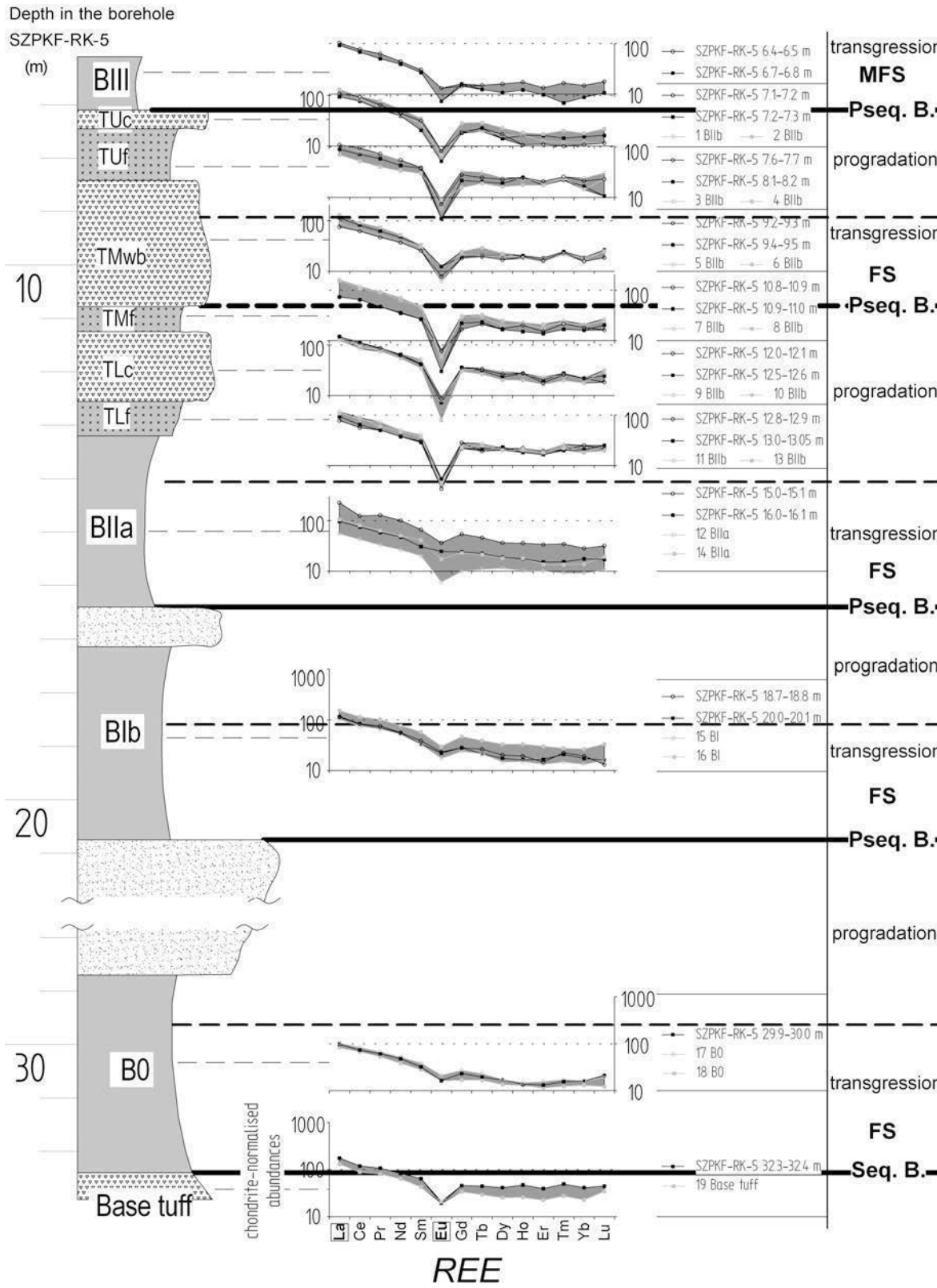

Figure 10. *REE* patterns from the borehole SZPKFRK-5 in considering their sequence stratigraphic status.

https://doi.org/10.1346/CCMN.2008.0560103 Published online by Cambridge University Press

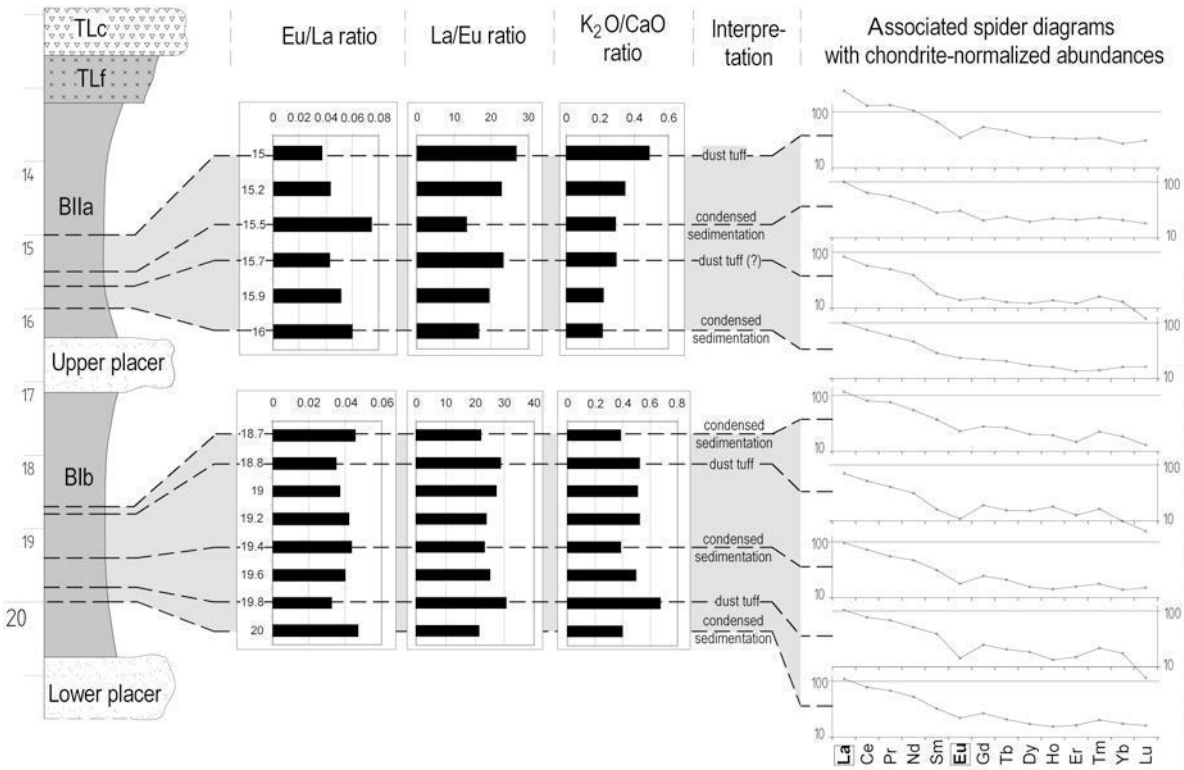

Figure 11. Microstratigraphic geochemical trends through some of the bentonite layers.

facies, are well defined as separable parasequences by the conventional interpretation (Van Wagoner *et al.*, 1990) of SP anomalies and resistivities (Figures 3, 9).

The volcanism-related cycles of the BIIb, characterized by the sudden increase in K_2O/CaO and La/Eu values at the base, can be traced in natural γ curves. A sudden increase in the natural γ activity can be seen at the TLf sub-unit followed by an upwards decreasing trend towards the TMwb (Figure 9). The natural γ reaches its next maximum at the TUf followed by another section with decreasing intensities upwards from there. The volcanic cycle starting with the TMf is detectable only by the geochemical proxies, presumably due to the limited changes in the K values.

CONCLUSIONS

A detailed stratigraphic and facies reconstruction of a bentonitized acid tuff succession, deposited within a Sarmatian, Upper Miocene transgressive systems tract named as the Ser-3 eustatic cycle, at Sajóbábony, northern Hungary, was performed *via* petrographic study and systematic mineralogical and geochemical analyses. The aim of the work was partly to test some proxies as indicators of the degree of alteration of the volcanogenic sediments and using these proxies to investigate the control of the relative volcanic sedimentation rate on the degree of weathering. The results can be summarized as follows:

(1) The synchronous changes of K_2O and CaO, together with the associated changes in Eu content, are demonstrated by correlations between CaO/K_2O and Eu/La ratios with $R^2 = 0.8$ and the saturation behavior of Eu incorporation. The saturation point of the Eu incorporation was determined to be [Eu*] = 1.25 ppm, which fits well with the associated chondrite-normalized *REE* patterns.

(2) The CaO/K_2O, Eu/La, and La/Eu ratios show correlation with the mineralogical changes, *i.e.* the montmorillonite/X-ray amorphous phase ratio with $R^2 = 0.59$, $R^2 = 0.72$, and $R^2 = 0.69$, respectively, suggesting Ca and Eu incorporation, associated with devitrification and smectite formation. This indicates that the level of alteration is closely correlated with the degree of alteration.

(3) In a sequence-stratigraphic context, the Ca content and the Eu/La values show local peaks and Eu anomalies characteristic of acid tuffs show minima at flooding surfaces. Within a bentonite layer, representing a single transgressive period, the repeated events of dust-tuff accumulations have been determined by K_2O/CaO and La/Eu peaks, confirmed also by the Eu anomalies in the *REE* patterns. Thus we conclude that the degree of alteration is closely correlated with the elimination of terrigenous input in the course of transgressive periods and a minimum in volcanic sedimentation rate due to dust-tuff accumulation allowing more intensive alteration of the deposited volcanic material.

https://doi.org/10.1346/CCMN.2008.0560103 Published online by Cambridge University Press

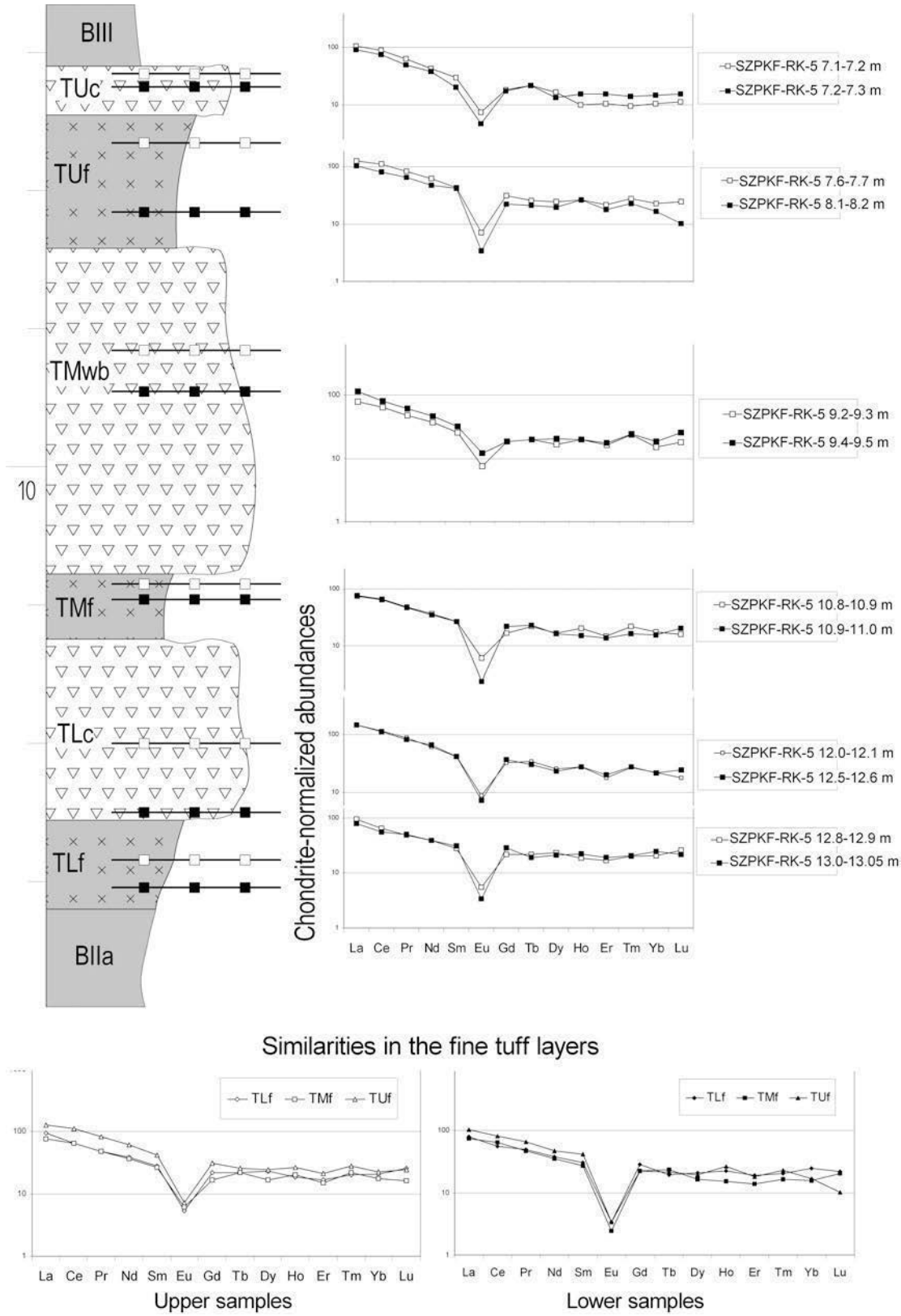

Figure 12. Chondrite-normalized *REE* patterns within subunits of the BIIb unit.

https://doi.org/10.1346/CCMN.2008.0560103 Published online by Cambridge University Press

(4) In the case of pumiceous tuffs, Eu anomalies in *REE* patterns reflect a limited alteration at the bottom, with more intensive alteration at the upper part of the fine tuff beds and an overall alteration in coarse tuff beds. This is interpreted as a result of infiltration of sea water into the pores of the tuff during the break in sedimentation, with more efficient infiltration in the case of the coarse tuffs. Another interpretation of the phenomena is that within a volcanic cycle ranging from the base of a 'fine' to the top of the subsequent 'coarse' sub-unit, a continuous decrease in volcanic sedimentation rate can be detected, *e.g.* due to the increasing accommodation space, associated with a more intensive effect of re-sedimentation.

ACKNOWLEDGMENTS

We thank the reviewers, especially Dr Charles Ver Straeten (New York State Museum, USA) for his painstaking work on our manuscript, considering both context and style. His detailed comments improved the final version significantly. We also thank Associate Editor, Professor Warren D. Huff (University of Cincinnati, USA).

REFERENCES

Allen, S.R. and McPhie, J. (2003) Phenocryst fragments in rhyolitic lavas and lava domes. *Journal of Volcanology and Geothermal Research*, **126**, 263–283.

Bartha, A. and Bertalan, É. (1997) Determination of the rare earth elements of rock samples by ICP-MS using different sample decomposition methods. *Acta Mineralogica-Petrographica, Szeged*, **38**, 131–149.

Bartha, A., Ballók, I., and Geoff, T. (2004) Simultaneous determination of mercury, hybridizing elements and those detectable by conventional pulverizing techniques by CMA-ICP-AES method. *Annual Report of the Geological Institute of Hungary for* **2002**, 55–68.

Bea, F. (1996) Residence of REE, Y, Th and U in granites and crustal protoliths; implications for the chemistry of crustal melt. *Journal of Petrology*, **37**, 521–552.

Bergström, S.M., Huff, W.D., and Kolata, D.R. (1998) The lower Silurian Osmundsberg K-bentonite. Part I: stratigraphic position, distribution, and paleogeographic significance. *Geological Magazine*, **135**, 1–13.

Bertalan, É., Bartha, A., Ballók, I., and Varga-Barna, Zs. (2003) The influence of experimental leaching conditions for the determinations of the soluble element content of soil and stream sediment samples. *International Journal of Environmental Analytical Chemistry*, **82**, 771–784.

Cant, D.J. (1992) Subsurface facies analysis. Pp. 27–46 in: *Facies Models* (R.G. Walker and N.P. James, editors). Geological Assocation of Canada.

Cullers, R.L., Chaudhuri, S., Arnold, B., Lee, M., and Wolf, C.W. (1975) Rare earth distributions in clay minerals and in the clay-sized fraction of the Lower Permian Havensville and Eskridge shales of Kansas and Oklahoma. *Geochimica et Cosmochimica Acta*, **39**, 1691–1703.

Curti, E., Kulik D.A., and Tits, J. (2005) Solid solutions of trace Eu(III) in calcite: thermodynamic evaluation of experimental data in a wide range of pH and pCO_2. *Geochimica et Cosmochimica Acta*, **69**, 1721–1737.

Fisher, R.V. and Schmincke, H.U (1984) *Pyroclastic Rocks*. Springer-Verlag, Berlin, 472 pp.

Gilbert, J.S. and Lane, S.J. (1994) The origin of accretionary lapilli. *Bulletin of Volcanology*, **56**, 398–411.

Hámor, G. (1997) Miocene palaeogeographic and facies maps of the Pannonian Basin. In: *Geological Maps of Hungary* **19**. Geological Institute of Hungary.

Haq, B.U., Hardenbol, J., and Vail, P.R., (1988) Mesozoic and Cenozoic chronostratigraphy and cycles of sea-level change. Pp. 71–108 in: *Sea-level Change: an Integrated Approach* (C.K. Wilgus, B.J. Hastings, H. Posamentier, J.C. van Wagoner, C.A. Ross and C.G. St. C. Kendall, editors). SEPM Special Publication **42,** Society for Sedimentary Geology, Tulsa, Oklahoma.

Harangi, Sz., Mason, P.R.D., and Lukács, R. (2005) Correlation and petrogenesis of silicic pyroclastic rocks in the Northern Pannonian Basin, Eastern-Central Europe: In situ trace element data of glass shards and mineral chemical constraints. *Journal of Volcanology and Geothermal Research*, **143**, 237–257.

Huff, W.D., Bergström, S.M., Kolata, D.R., and Sun, H. (1997a) The Lower Silurian Osmundsberg K-bentonite. Part II: Mineralogy, geochemistry, chemostratigraphy and tectonomagmatic significance. *Geological Magazine*, **135**, 15–26.

Huff, W.D., Morgan, D.J., and Rundle, C.C. (1997b) *Silurian K-bentonites of the Welsh Borderlands: Geochemistry, mineralogy and K-Ar ages of illitization*. British Geological Survey, Report WG/96/45, 25 pp.

Huff, W.D., Bergström, S.M., and Kolata, D.R. (2000) Silurian K-bentonites of the Dnestr Basin, Podolia, Ukraine. *Journal of the Geological Society, London*, **157**, 493–504.

Juvonen, R., Bartha, A., Lakomaa, T., Soikkeli, L., Bertalan, E., Kallio, E., and Ballók, M. (2004) Comparison of recoveries by lead fire assay and nickel sulphide fire assay in the determination of gold, platinum, palladium and rhenium in sulphide ore samples. *Geostandards Newsletter*, **28**, 123–130.

Klug, H.P. and Alexander, L.E. (1954) *X-ray Diffraction Procedures*. John Wiley Sons Inc., New York-London-Paris, 716 pp.

Kolata, D.R., Huff, W.D., and Bergström, S.M. (1998) Nature and regional significance of unconformities associated with the Middle Ordovician Hagan K-bentonite complex in the North American mid-continent. *Geological Society of America Bulletin*, **110**, 723–739.

Lakshtanov, L.Z. and Stipp, S.L.S. (2004) Experimental study of Europium (III) coprecipitation with calcite. *Geochimica et Cosmochimica Acta*, **68**, 819–827.

MacRae, N.D., Nesbitt, H.W., and Krinberg, B.I. (1992) Development of a positive Eu anomaly during diagenesis. *Earth and Planetary Science Letters*, **109**, 585–591.

Min, K., Renne, P.R., and Huff, W.D. (2001) $^{40}Ar/^{39}Ar$ dating of Ordovician K-bentonites in Laurentia and Baltoscandia. *Earth and Planetary Science Letters*, **185**, 121–134.

Náray-Szabó, I., Zsoldos, L., and Kálmán, A. (1965) *Introduction to XRD Structure Investigation* (in Hungarian). Association of Hungarian Chemists, Budapest, 305 pp.

Nash, W.P. and Crecraft, H.R. (1985) Partition coefficients for trace elements in silicic magmas. *Geochimica et Cosmochimica Acta*, **49**, 2309–2322.

Pearce, N.J.G., Westgate, J.A., Perkins, W.T., and Preece, S.J. (2004) The application of ICP–MS methods to tephrochronological problems. *Applied Geochemistry*, **19**, 289–322.

Pécskay, Z., Balogh, K., Széky, F.V. and Gyarmati, P. (1987) K/Ar geochronology of the Miocene volcanism in the Tokaj Mountains (in Hungarian). *Bulletin of the Geological Society of Hungary*, **117**, 237–253.

Pécskay, Z. and Molnár, F. (2002) Relationships between volcanism and hydrothermal activity in the Tokaj Mountains, North-east Hungary. *Geologica Carpathica*, **53**, 303–314.

Pellenard, P., Deconinck, J.F., Huff, W.D., Thierry, J., Marchand, D., Fortwengler, D., and Trouiller, A. (2003) Characterization and correlation of Upper Jurassic (Oxfordian) bentonite deposits in the Paris Basin and the Subalpine Basin, France. *Sedimentology*, **50**, 1035.

Püspöki, Z. (2002) Miocene development of the Tardona Hills in relation to the facies and stratigraphic data of sediment sequences. PhD thesis, University of Debrecen, Hungary, 128 pp.

Püspöki, Z., Kozák, M., Kovács-Pálffy, P., Földvári, M., McIntosh, R.W., and Vincze, L. (2005) Eustatic and tectonic/volcanic control in sedimentary bentonite formation – a case study of Miocene bentonite deposits from the Pannonian Basin. *Clays and Clay Minerals*, **53**, 71–91.

Rischák, G. (1989) Direct XRD determination of amorphous phase in rocks and soils (in Hungarian). *Annual Report of the Geological Institute of Hungary for 1987*, 377–394.

Rischák, G. and Viczián, I. (1974) Factors influencing the base reflection intensity of clay minerals (in Hungarian). *Annual Report of the Geological Institute of Hungary for 1972*, 229–256.

Sene, J. (1967) Chronostratigraphie und Neostratotypen. Miozän M_3, Miozän der Zentralen Paratethys. *Vydavatelstvo Slovenskej Akademie Vied*, Bratislava, pp. 1–312.

Tits, J., Wieland, E., Bradbury, M.H., Eckert, P., and Schaible, A. (2003) *The Uptake of Eu(III) and Th(IV) by Calcite under Hyperalkaline Conditions*. PSI Report 02–03, Paul Scherrer Institute, Villigen, Switzerland.

Vakarcs, G., Hardenbol, J., Abreu, V.S., Vail, P.R., Várnai, P., and Tari, G. (1998) Oligocene–Middle Miocene depositional sequences of the Central Paratethys and their correlation with regional stages. Pp. 209–231 in: *Mesozoic and Cenozoic Sequence Stratigraphy of European Basins* (P.-C.D. Graciansky, J. Hardenbol, T. Jacquin, and P.R. Vail, editors). SEPM Special Publication, **60**, Society for Sedimentary Geology, Tulsa, Oklahoma.

Van Wagoner, J.C., Mitchum, R.M., Campion, K.M., and Rahmanian, V.D. (1990) Siliciclastic sequence stratigraphy in well logs, cores, and outcrops: concepts for high-resolution correlation of time and facies. *AAPG Methods in Exploration*, Series **7**, 55 pp., American Association for Petroleum Geologists, Tulsa, Oklahoma.

Ver Straeten, C.A. (2004) K-bentonites, volcanic ash preservation, and implications for Early to Middle Devonian volcanism in the Acadian orogen, eastern North America. *GSA Bulletin*, **116**, 474–489.

Yasumasa, O., Naotatsu, S., Daizo, I., Hinako, S., and Toshio, M. (2005) An experimental study on felsic rock–artificial seawater interaction: implications for hydrothermal alteration and sulfate formation in the Kuroko mining area of Japan. *Mineralium Deposita*, **39**, 813–821.

Zhong, S. and Mucci, A. (1995) Partitioning of rare earth elements (REEs) between calcite and seawater solutions at 25ºC and 1 atm, and high dissolved REE concentrations. *Geochimica et Cosmochimica Acta*, **59**, 443–453.

(*Received 7 June 2006; revised 24 July 2007; Ms. 1180; A.E. Warren D. Huff*)